Vibrations in materials with granularity

Zeravcic, Z.

Citation

Zeravcic, Z. (2010, June 29). *Vibrations in materials with granularity*. *Casimir PhD Series*. Retrieved from https://hdl.handle.net/1887/15754

Chapter 3

Localization in Granular Packings

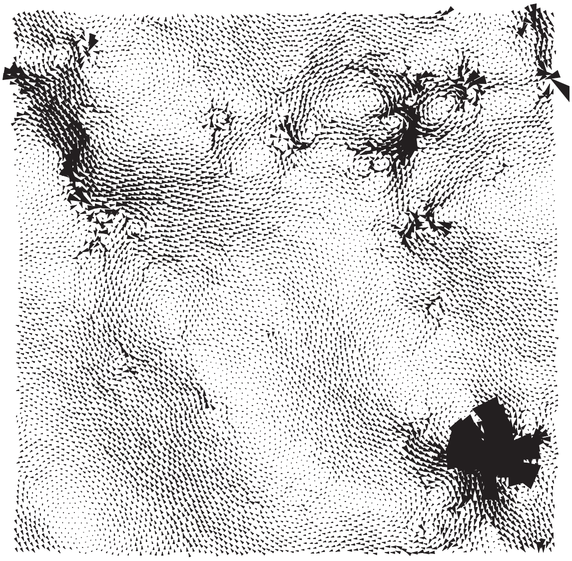

3.1 Introduction

As introduced in Section 1.2.1, many questions concerning the behavior of disordered systems have been put in a new perspective by addressing them from the point of view of the more general jamming scenario [85]. Especially for granular systems it has turned out to be very fruitful to study the changes in the properties and the response of granular packings as one approaches the jamming point, where the packing gets close to an isostatic solid from the jammed side.

In Section 1.2.3, an isostatic packing is introduced as a marginal solid which has just enough contacts to maintain stability. The average coordination number Z of a d-dimensional isostatic packing of frictionless spheres equals $Z_{\text{iso}} = 2d$ [84] (see Subsection 1.2.3). Upon approaching this marginal solid, many static and dynamic properties exhibit anomalous behavior, associated with the fact that the excess number of average bonds, $\delta Z = Z - Z_{\text{iso}}$, goes to zero [7,28,54,55]. As explained in Section 1.2.1, δZ itself scales anomalously (as the square root of the difference in density from the one at jamming, $\phi - \phi_c$, [7]), the ratio G/K of the shear modulus G over the compression modulus K is found to scale as δZ, and the Debye scaling of the low-frequency part of the density of states breaks down. Moreover, $D(\omega)$ becomes flat at low frequencies above some crossover frequency $\omega^* \sim \delta Z$, due to an excess density of low frequency modes.

Much of this behavior was explained by Wyart *et al.* [28,54,55] in terms of the existence of an important cross-over length scale $\ell^* \sim 1/\delta Z$, the length up to which the response is close to that of an isostatic packing (for details see Subsection 1.2.2). This scale ℓ^* diverges as the jamming point is approached, but is difficult to probe directly. Nevertheless, the length ℓ^* has recently been uncovered as the important cross-over length to continuum behavior in the static response [98]. Although most of these results pertain explicitly to packings of frictionless spheres, as we saw in Chapter 2 and as can be found in [76,101,103], many of these ideas can be extended and applied to ellipsoidal and frictional packings respectively, and are relevant for glasses as well [34,36]. The ellipsoidal case is studied in Chapter 2.

In this Chapter we are going to address another aspect of the vibrational modes. It has been noted in several studies that both the response to a local or global deformation [98,104] and the behavior of the vibrational eigenmodes [28,54] of a packing become much more disordered as one approaches the jamming point: as the snapshots of two low frequency vibrational modes in Fig. 3.1 illustrate, far above the jamming point the eigenmodes have a structure reminiscent of what is observed in a continuum theory of an elastic medium, but close to the jamming point one is immediately struck by the appearance of many disordered "swirls". The arguments put forward by Wyart *et al.* [28,54,55] indicate that the excess low frequency modes cannot be localized on scales $\lesssim \ell^*$ since they are the vestiges of the *global* floppy modes that emerge at the isostatic point. Hence, if there are any low-frequency modes away from jamming, and if indeed their localization length is $\gtrsim \ell^*$, we should be able to see this length changing as the jamming point is approached. This Chapter is dedicated to investigating whether that is the case.

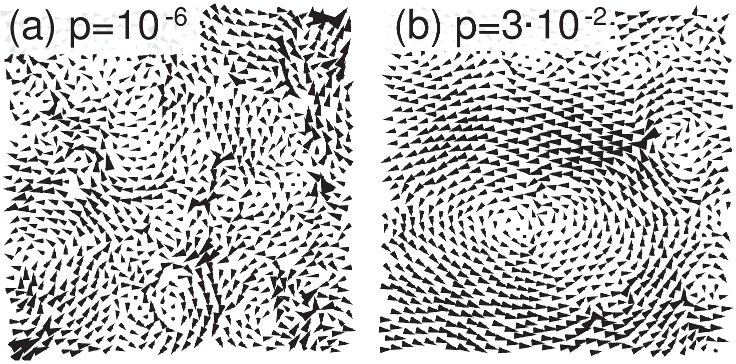

Figure 3.1: Snapshots of two low-frequency eigenmodes in our packings. The arrows indicate the direction and magnitude of the displacements of the individual particles. (a) At low pressure $p = 10^{-6}$, close to the jamming point, the mode is very disordered, whereas at high pressure (b) $p = 3 \cdot 10^{-2}$, the mode is more reminiscent of an elastic shear wave. Similar features are seen in the response to a local or global deformation [54, 98, 104].

3.1.1 Reminder on localization

Localization was discovered fifty years ago by Anderson [4], who in his study of non-interacting electrons in a random potential found that disorder can induce electron localization. Unlike the extended (delocalized) Bloch waves, in a localized state the weight of the electron wave function is concentrated near some point in space; the amplitude falls off as $e^{-r/\xi}$ with distance r from the center. This defines the localization length $\xi(E)$ which depends on the electron energy E. The possibility that disorder can localize the eigenmodes of systems governed by wave equations is quite general and extends to many systems, including sound modes [2, 5, 105] and also gravity waves [2], light propagation [2] and diffusion on random lattices [2, 105]. Generally speaking, in one and two dimensions there is no localization-delocalization transition: *in the thermodynamic limit*, for any amount of disorder, all the states are localized. In this Chapter we will focus on the localization behavior of vibrational modes of $2d$ frictionless packings.

3.1.2 Types of disorder

The dynamic response of granular packings is affected by three types of disorder — bond disorder, mass disorder and geometric packing disorder. As we shall show through various examples, any of these types is sufficient to cause localization in our finite systems, and in practice, for realistic models of granular packings all three play a role. Bond disorder is present for all force laws except one-sided harmonic springs, polydisperse particles will have varying masses, and geometric disorder is naturally present except for especially prepared regular piles, like a regular stack of marbles. Of course, in computer models these effects can be separated easily. In this Chapter we will first address localization properties of vibrational modes in $2d$ granular packings, and then try to attempt to disentangle these three contributions through studying simpler systems, and use this to our advantage in testing our scaling predictions of the localization length with the amount of disorder (Section 3.6).

3.1.3 Outline

The crucial dilemma in extracting the localization length of the vibrational modes of granular packings is that the effective disorder is so weak that one needs prohibitively large systems to reach the true localization regime $\xi \ll L$ for most modes. (Here L is the linear system size.) At the same time, existing methods which are based on spatial averages (like the direct expression based on the second moment of the eigenmode or the (Inverse) Participation Ratio method [106]) do not give much insight into the structure of the modes when ξ approaches the system size L. More precisely, all conventional methods essentially yield the same localization length in the localization regime $\xi \ll L$, while for modes which are extended throughout the finite system one finds $\xi \approx L$.

The method we introduce in this Chapter, which is motivated by earlier work on non-Hermitian quantum problems [107, 108], is based on studying the response to an asymmetric perturbation. It not only gives the proper localization length ξ of each localized mode (see Fig. 3.5), but at the same time assigns a well-defined and precise direction-dependent value $\xi(\phi)$ to each mode, that spans through our finite system (see Fig. 3.3). For our method, one can also extract useful information about the large system limit from studying the regime $\xi \gtrsim L$ and the scaling with the disorder, which opens up the possibility to bring Random Matrix Theory [106, 109] to bear on this class of problems.

This Chapter is organized as follows: First we will introduce in more detail our method and explain how we extract the localization length. This is followed by a short Section on the description of our packings and with a reminder on the $D(\omega)$ for these systems. In Section 3.4 we will present our results for the case of $2d$ granular packings on which we focus in this Chapter the most. This is followed by a Section on the Random Matrix Theory and its tools, that we successfully use to prove scaling behavior we find. The last Section is devoted to exploring our method through studying simple $1d$ and $2d$ model systems, where we can disentangle different types of disorder.

3.2 Method

Our method to extract the localization length is motivated by the work of Nelson and Hatano [107, 108], on the delocalization transition in non-Hermitian transfer matrix problems arising in the statistical mechanics of vortex lines in superconductors. To illustrate this method consider first the case of a one-dimensional chain of masses connected by springs with spring constants k_{ij} ($j = i \pm 1$) and periodic boundary conditions. We introduce an asymmetric bias term into the equations of motion so that the eigenvalue equation of a mode $u_i e^{-i\omega t}$ becomes:

$$m_i \omega^2 u_i = \sum_{j=i\pm 1} k_{ij} \left(e^{h\hat{x}\cdot\vec{x}_{ij}} u_j - u_i \right). \tag{3.1}$$

Here x_i are the rest positions of the particles and $\vec{x}_{ij}$ is a vector pointing from particle i to particle j. For $h = 0$ this is simply the dynamical equation for vibrations. The trick now is that we can extract the localization length ξ_k of each mode k by following whether or not its eigenvalue ω_k^2 changes when we turn on h in small steps. Indeed, as long as $h < 1/\xi_k$ the eigenvalue ω_k^2 will not change at all. To see this, note that in this case we can perform a "gauge transformation" to a field $\tilde{u}_i = u_i e^{hx_i}$ which obeys the original equation with $h = 0$ *and* which falls off exponentially on both sides so that, in a large enough system, it obeys the periodic boundary conditions. This implies that for $h < 1/\xi_k$, the eigenvalue ω_k^2 does not change. However, once $h > \xi_k$ the function $\tilde{u}$ obtained with this transformation does not fall off exponentially to both sides. Thus, it cannot obey the periodic boundary condition with the same eigenvalue as it had for $h < 1/\xi_k$: its eigenvalue *has* to change! In practice, when we increase h the eigenvalue ω_k^2 starts to change rapidly and collide with a neighboring eigenvalue when $h \approx 1/\xi$; beyond that, when $h \gtrsim 1/\xi_k$ the eigenvalue ω_k^2 moves into the complex plane [107, 108]. Hence we can simply obtain the localization length ξ_k of each mode k from the value h_k at which the eigenvalue moves into the complex plane upon increasing h: $\xi_k = 1/h_k$.

It is straightforward to extend this method to higher dimensions: as above, we simply multiply the off-diagonal elements of our dynamical matrix with an exponential $e^{\vec{r}_{ij}\cdot\vec{h}}$, where $\vec{r}_{ij}$ is the vector pointing from the center of particle i to its neighbor j. Our probe field $\vec{h}$ is now a vector, so by changing the angle that $\vec{h}$ makes with the x-axis, we can extract the angular anisotropy of the localization length $\xi(\phi)$ of each mode.

3.3 Granular packings and $D(\omega)$

We use $2d$ packings of 1000 frictionless particles which are prepared using molecular dynamics simulations — see [31, 76, 98] for the description of our algorithm, which gently prepares packing at a target pressure, as well as for other details. The particles interact with the $3d$ Hertzian force law, $f_{ij} \simeq \delta_{ij}^{3/2}$, where δ_{ij} is the overlap between particles i and j. The unit of length is the average particle diameter. Unless noted otherwise we here present results for our most extensive studies with 20% polydispersity in the radii. Runs with different amount of polydispersity give similar results. The masses m_i of the grains are taken proportional to R_i^3, corresponding to packing of spheres in $2d$. The confining pressure, with which we tune the distance from the jamming point, is in the range $p \in (10^{-6}, 3 \cdot 10^{-2})$ in the units of the Young modulus of the particles. We employ periodic boundary conditions in both directions.

Our use of the $3d$ Hertzian force law implies that the vibrational bond strengths $k_{ij} = df_{ij}/d\delta_{ij} \sim \delta_{ij}^{1/2} \sim p^{1/3}$ are disordered (they vary from bond to bond) and get weaker at smaller pressures. The natural frequency scale therefore goes down with pressure as $p^{1/6}$. As in previous studies [76], when reporting our data we will always rescale all frequencies ω with a factor $p^{-1/6}$, as to be able to compare data at different pressures.

The vibrational modes and their density of states ($D(\omega)$ or DOS) are obtained in the standard way, by expanding the energy about the equilibrium positions of the grains up to quadratic terms. Just as in solid state physics (see Section 1.1.1), the dynamical matrix, whose elements are the second derivatives of the energy with respect to the positions of the grains, determines the linear equations of motion of the vibrational modes. The dynamical matrix of a granular packing is a sparse symmetric matrix, because each particle only interacts with a few others.

In Fig. 3.2 we show that the density of states of our packings behaves as found before [7, 28, 54, 55, 76] for such packings: As the the jamming point is approached by lowering the pressure, the density of low-frequency modes increases dramatically, which, as mentioned before, is due to the nearness of the isostatic point. Representative examples of modes from the spectrum of very compressed packing are shown in Fig. 3.2(1-4). The modes in the low-frequency range, Figs. 3.2 (1) and (2), are like a plane-wave or consist out of a high-amplitude motion of a few particles, coupled to a continuum structure. The amplitude of the modes in the high -frequency range, Fig. 3.2(4) is practically localized on a few particles in the packing. The rest of the modes in the spectrum, especially those of packings close to the jamming point, are spanning the system and have very disordered, swirly appearance, as captured by Fig. 3.2(3).

3.4 Measuring the localization length ξ

In this Section we will start with a systematic analysis of our data, obtained using the method described in Section 3.2. We first discuss some properties of the localization length of individual modes before turning to their scaling as a function of frequency, system size and distance from the jamming point.

3.4.1 Anisotropy and spread

As we already introduced, our method allows us to study angular dependence of the localization length. Fig. 3.3 shows the angular dependence $\xi(\phi)$ of a few typical modes, for two different pressures. One clearly sees that $\xi(\phi)$ is a π-periodic function and that the angular variation of $\xi(\phi)$ is significant.

While few modes, like ones in Figs. 3.3(c) and (g), have a quadrupolar structure, the anisotropy is predominantly dipolar, as the histogram in Fig. 3.3(h) shows. Fig-

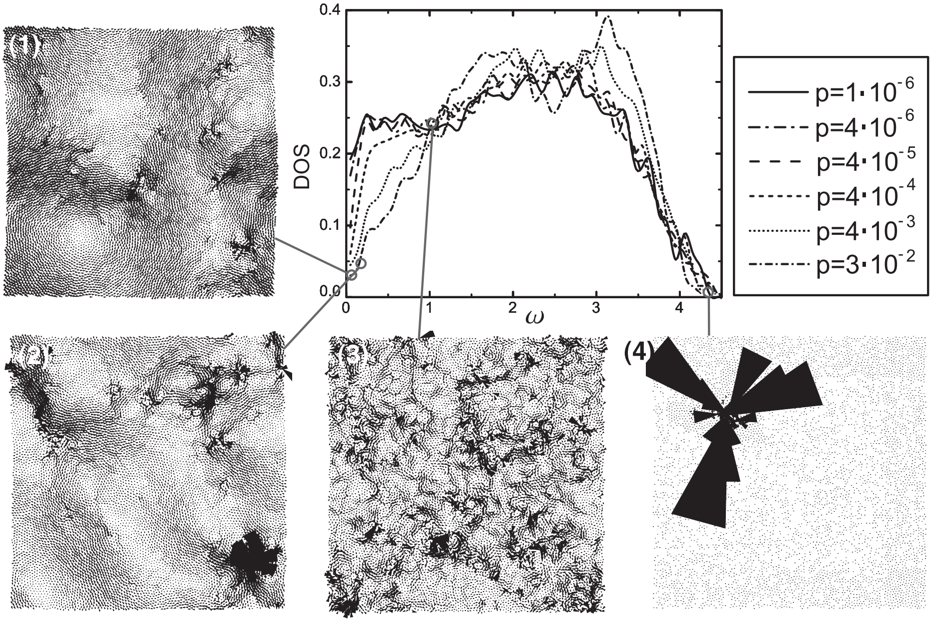

Figure 3.2: $D(\omega)$ of our 1000 particle packings for 6 different pressures confirming the main features of earlier studies close to jamming, [7, 28, 54, 55, 76]. (1-4) Typical modes for the system of 10000 particles and pressure $p = 3 \cdot 10^{-2}$: (1) Plane-wave like lowest frequency mode, (2) Quasi-localized low-frequency mode (see main text for details), (3) Disordered mid frequency mode and (4) High-frequency mode localized within the system size. We should note that the pattern of mode (3) is also typical for the modes in the plateau of $D(\omega)$ of systems close to the point J.

ure 3.4 shows that the root mean square average angular variation $\Delta\xi$ of $\xi(\phi)$ is almost half ξ, and that it is slightly larger at higher frequencies. There is no strong dependence of the anisotropy on the pressure, *i.e.*, on the distance from the jamming point.

The angularly averaged values $\xi(\omega)$ show also a large spread, as Fig. 3.5 illustrates for a small value of the pressure. One also sees from this figure that most modes have a value of $\xi \gtrsim L$, which means that they are extended within the systems we can analyze — only our largest frequency modes are truly localized [34, 36, 110]. We will denote from here on the angularly averaged value of the localization length of an individual mode by ξ.

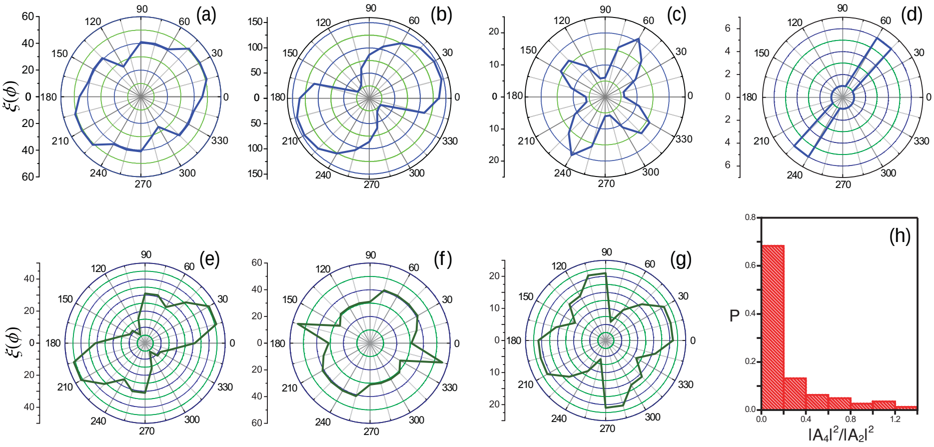

Figure 3.3: Polar plots of the localization length $\xi(\phi)$ in two of our granular packings: *(i)* at $p = 4\cdot10^{-4}$ at low in (a), intermediate in (b-c), and high frequency in (d), and *(ii)* at $p = 1\cdot10^{-6}$ at low in (e), intermediate in (f), and high frequency in (g). The angular variation of $\xi(\phi)$ is comparable to the angularly averaged value itself. (h) Histogram of the ratio of squared amplitudes of the fourth (quadrupole) and second (dipole) harmonic at $p = 4\cdot10^{-4}$. Note how most modes have predominantly dipole symmetry.

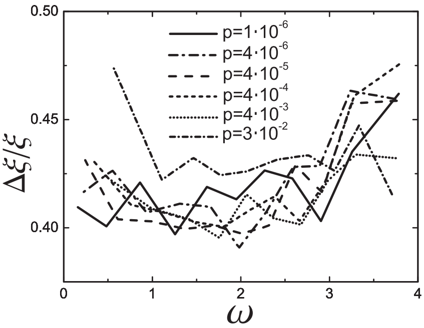

Figure 3.4: Average angular anisotropy $\Delta\xi/\bar{\xi}$ as a function of frequency for various pressures.

3.4.2 Frequency bin-averaged localization length $\bar{\xi}(\omega)$

We stress that although we will follow common practice in referring to ξ as the *localization* length even for $\xi \gtrsim L$, one should keep in mind that many modes *extend* throughout our finite periodic system, as both Figs. 3.5, 3.2 and 3.3 illustrate.

For each dataset of the individual angularly averaged values of ξ, as in Fig. 3.5, we determine the frequency binned average values $\bar{\xi}(\omega)$ (each based on about 100

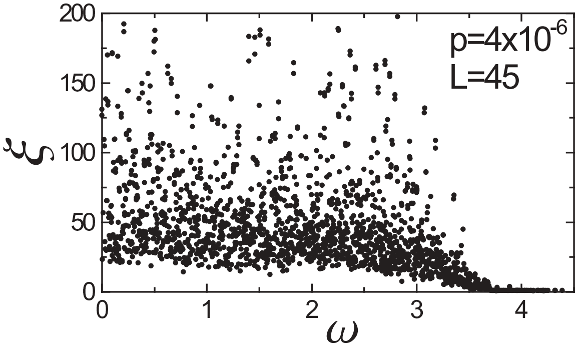

Figure 3.5: Scatter plot of the angularly averaged ξ's of all the 2000 modes of our granular packing of 1000 particles as a function of the frequency ω at pressure $p = 4 \cdot 10^{-6}$ studied with the method explained in the text. Note the large scatter and the fact that the ξ values are of order of the linear system size $L = 45$ or larger throughout most of the frequency range.

to 200 modes). The behavior of $\bar{\xi}/L$ as a function of (scaled) frequency is shown in Fig. 3.6(a) for six different values of the pressure. In these average values, there is no strong variation with pressure, *i.e.*, with distance to jamming.

We already noted in Fig. 3.5 that most of our eigenmodes have $\xi \gtrsim L$, *i.e.*, are extended in our finite system. This is also clear from Fig. 3.6(a): at all but the largest frequencies we have, $\bar{\xi} \gtrsim L$. There are indeed roughly three regimes present in Fig. 3.6(a). From high frequencies towards low frequencies, we first have a range of high-frequency localized modes, for which $\bar{\xi} < L$. These modes are always present at any pressure and are the high-frequency modes in which only a few (light) particles oscillate more or less in anti-phase as in an optical mode (such type of modes generally arise immediately when disorder is introduced into an ordered system), see Fig. 3.2(4). For intermediate-range frequencies there is a plateau in $\bar{\xi}$, and a representative of a mode in this frequency range is shown in Fig. 3.2(3). Finally for the lowest frequencies (in the frequency range where actually the excess modes appear in the $D(\omega)$ in Fig. 3.2 at low pressures), there is an indication of an upswing in $\bar{\xi}$ for small ω. Modes depicted in Fig. 3.2(1-3) are good representatives of types of modes appearing in the low-frequency part of the spectrum of our packings, though the plane-wave like mode, depicted in Fig. 3.2(1), shows up only in the spectrum of sufficiently large systems.

Plots (b) and (c) in Fig. 3.6 show histograms of distances between energy levels of our packings. We find that the low frequency modes are extended, following the so-called Wigner conjecture, where as high frequency modes are Anderson localized with non-interacting level spacings (*i.e.*, spacings follow a Poisson distribution). For more details see Section 3.4.5, where we discuss Level Spacing Statistics.

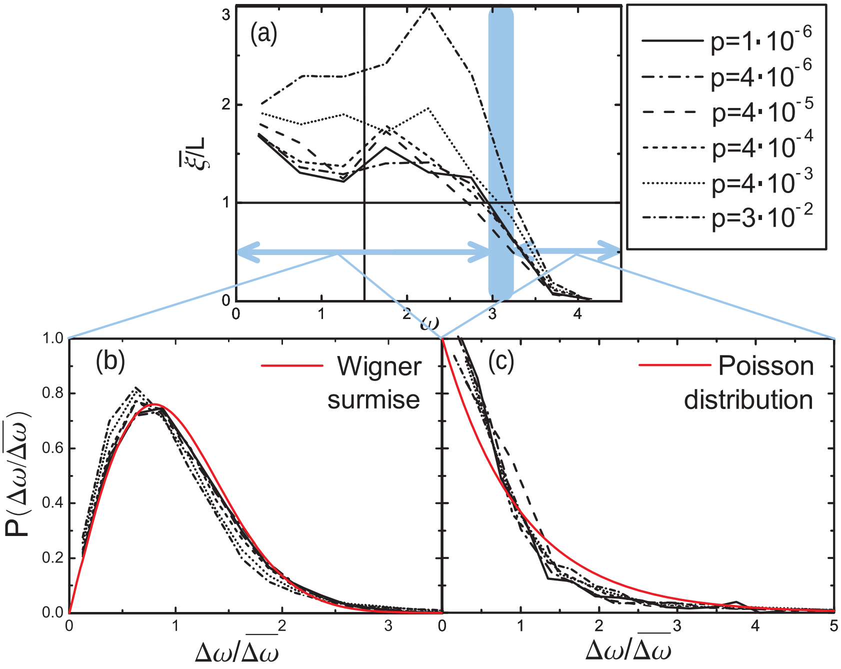

Figure 3.6: (a) Frequency binned and angularly averaged values of $\bar{\xi}(\omega)/L$ for different pressures. Note how the general trend does not depend in the distance to the jamming point: modes in the very high-frequency end of the spectrum have $\bar{\xi} \lesssim L$, whereas the rest of the modes are extended, with $\bar{\xi} \gtrsim L$. (b,c) Level spacing statistics for the modes that have $\bar{\xi} \gtrsim L$ in (c) and for the modes with $\bar{\xi} \lesssim L$ in (b). The lower frequency modes are essentially all extended and do show level repulsion in accord with the predictions from Random Matrix Theory [106, 109] (see Section 3.4.5), while the high frequency modes are truly localized and their level spacing is close to Poissonian. The red lines indicate the frequency ranges used to obtain the level statistics in (b) and (c) (for connection with the Random Matrix Theory see Sections 3.4.5 and 3.5).

3.4.3 Quasi-localized low-frequency modes at high pressure

From Fig. 3.6(a) of the bin-averaged $\bar{\xi}$, it would appear *at first sight* that we see no signature of the nearness of the jamming point. This, however, is not true: in Fig. 3.6 we show data obtained by averaging over 100-200 modes. However, this averaging washes out systematic trends visible for the lowest frequency eigenmodes discovered by Vitelli, Xu *et al.* [34, 36]. When plotted on a logarithmic scale, as in Fig. 3.7, we see a systematic trend for ξ of the low frequency modes to decrease with increasing pressure. As the inset of Fig. 3.7(a) illustrates, these are "quasi-localized" modes in which a reasonably well defined "localized" group of particles performs what looks like a resonant oscillation that is weakly coupled to the extended elastic field. For our limited range of L, we find $\xi/L \simeq 0.3$ and a reduced anisotropy of $\Delta\xi/\xi \approx 0.2$ for these modes.

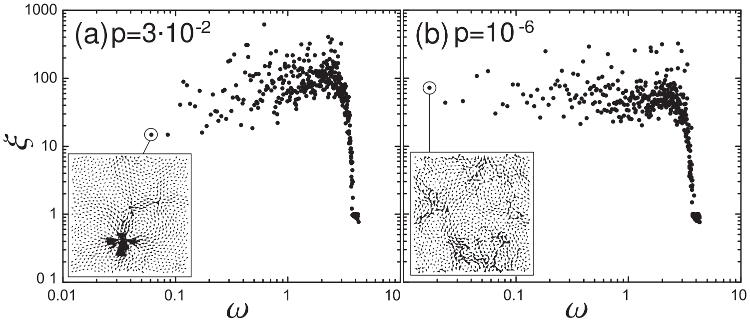

Figure 3.7: Scatter plot for the localization lengths ξ (determined to a precision of order unity) on a logarithmic frequency scale at $p = 3\cdot 10^{-2}$ in (a) and $p = 10^{-6}$ in (b) at system size $L = 45$. Note that at the large pressure the lowest-frequency modes are localized; at small pressures this is not the case. The inset illustrates the two lowest-frequency modes, which has $\xi/L \approx 0.3$ in (a) and $\xi/L \approx 2$ in (b).

As we discussed in the Introduction of this Chapter, for packings closer to the jamming point (at lower pressures) the isostaticity length ℓ^* increases as $1/\delta Z$, where δZ is the excess contact number. Up to this scale ℓ^* we do not expect localized modes at low frequencies, since up to this scale the response mirrors that of the *global* floppy modes that emerge near the isostatic point. Indeed, within the system sizes we can study there are no low-frequency "quasi-localized" modes at all at low pressures, as Fig. 3.7(b) illustrates for $p = 10^{-6}$, even though the response is in many ways more disordered due to the nearness of the jamming point!

While our data are qualitatively in accord with the above scenario, we have unfortunately too few low-frequency "quasi-localized" modes to confirm quantitatively that as we tune the packings closer to jamming, the extent of the resonant region increases with $\ell^* \sim 1/\delta Z$.

3.4.4 Distribution of large ξ

We also looked at the distribution of large ξ for systems with different pressure, and we found that this distribution has a power-law tail that goes like ξ^{-3}, regardless of the pressure or system size, Fig. 3.8. This scaling will be revisited in Section 3.5.

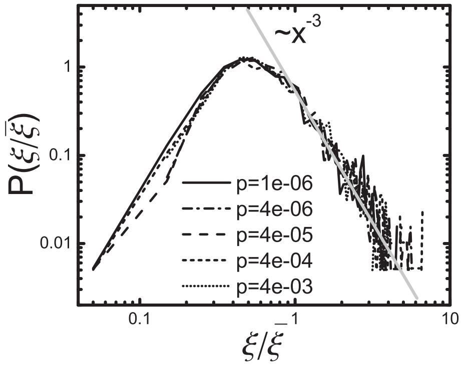

Figure 3.8: Log-log plot of the distribution of ξ's for different pressures; gray line shows the power law decay.

3.4.5 Level spacing statistics

The question that we want to ask here, that will be a nice segue for the next Section, is the following: is there an effect of the mode localization on the spectrum? Based on the results of Random Matrix Theory (RMT) [106, 109], one expects the following behavior: the frequencies ω_i of the localized modes should be independently distributed, so that their spacing $\Delta\omega_i = \omega_{i+1} - \omega_i$ obeys a Poisson distribution, while the modes which extend throughout the system should interact and repel each other, with a level spacing distribution which is given by the Wigner surmise, $P_W(s) = \pi s/2 \exp(-\pi s^2/4)$, where $s = \Delta\omega/\overline{\Delta\omega}$. Figs. 3.6(b,c) confirm that this expectation is fully born out by our data at all pressures. Note that the distribution in Fig. 3.6(b) deviates somewhat from the Wigner surmise at the two highest pressures — this is, we believe, due to the "quasi-localized" low-frequency modes discussed above.

These results motivate a more detailed analysis of implications of RMT on the problem at hand. Therefore we dedicate the following Section to a short exposition of relevant details of RMT, and the useful insights that it offers.

3.5 Implications from Random Matrix Theory

We will start from relating Random Matrix Theory (RMT) to our vibrational problem. Namely, the dynamical matrix $\hat{D}$ of our granular packing satisfies the conditions that a *real random matrix* should satisfy in order to belong to the so-called Gaussian Orthogonal Ensemble (GOE). The general conditions[1] are that $\hat{D} = \hat{D}^{\mathrm{T}}$, $\overline{D_{ij}} = 0$ and

---

[1] These conditions are derived for $N \times N$ random matrices, but are valid for sparse matrices if the mean number of non-zero elements per row or column is larger than some threshold value which is typically

$\overline{|D_{ij}|^2} = 1/N$ [106].

In order to analyze the energy levels of a random matrix like this, one must first check if the spectrum is homogeneous on energy scales exceeding a certain minimal range. However, if this is not the case, one has to do an *unfolding* of the spectrum [106]. Since we have that the density of the eigenvalues, *i.e.*, ω_i^2, of our dynamical matrix $\hat{D}$ is not homogeneous, we have to perform the unfolding procedure. This procedure is however not unique! One of natural ways to do this is as follows: We need to find a function $f(E_i)$ such that the rescaled levels $e_i = f(E_i)$ have mean spacing $1/N$, the mean evaluated with respect to energy intervals $[E - \Delta E/2, E + \Delta E/2]$. The corresponding rescaled interval goes from $f(E - \Delta E/2)$ to $f(E + \Delta E/2)$. We proceed with the following sequence of equalities:

$$\begin{aligned} \frac{1}{N} = \frac{\Delta e}{\Delta N} = \frac{1}{\Delta N}[f(E + \Delta E/2) - f(E - \Delta E/2)] \\ = \frac{\Delta E}{\Delta N} f'(E) = \frac{f'(E)}{\bar{\rho}(E) N} \end{aligned} \tag{3.2}$$

where we used the definition for bin averaged level density $\bar{\rho}(E) = \Delta N/(N\Delta E)$. After integrating the above equation, one gets that the function $f(E)$ is actually a bin averaged level staircase (staircase definition is $\sigma(E) = 1/N \sum_i \Theta(E - E_i)$, with Θ being the Heaviside function). For our case this function is proportional to the square root function, which then gives us an unfolded spectrum proportional to the density of *frequencies* instead of *frequencies squared*.

We can proceed with analyzing the Level Spacing Statistics (LSS) of our unfolded spectrum. Our results shown in Fig. 3.6(b) show that the modes, with localization length larger than the system size, repel each other since their behaviour follows the Wigner surmise:

$$P_W(s) = \frac{\pi}{2} s \exp\left(-\frac{\pi}{4} s^2\right) \tag{3.3}$$

where $s = \Delta\omega^2/\overline{\Delta\omega^2}$, $\Delta\omega^2$ is the level spacing and $\overline{\Delta\omega^2}$ is the average level spacing. Actually, we should write $\Delta\omega/\overline{\Delta\omega}$ now, since we are studying the unfolded spectrum. As it turns out, for our system it doesn't matter because we can write that $\Delta\omega^2 \sim 2\omega_{typ}\Delta\omega$ and $\overline{\Delta\omega^2} \sim 2\overline{\omega}\,\overline{\Delta\omega}$ so $\Delta\omega^2/\overline{\Delta\omega^2} \sim \Delta\omega/\overline{\Delta\omega}$). Once we introduce a non-zero value of the perturbation parameter $\vec{h}$, we know that modes start to shift and collide, which makes them "pop up" into the complex plane. This of course influences the level spacing statistics! We numerically checked this: Fig. 3.9 shows how the Wigner-like distribution transforms towards a Poisson-like one (it does not manage to transform completely because the modes pop into the complex plane rather *quickly*, *i.e.*, for small values $|\vec{h}|$). This change of the behavior of energy levels, with a change of a perturbation parameter, is a well known phenomena [111] — *e.g.*, the inset of Fig. 3.9 shows how the level spacing statistics of a hydrogen atom in a magnetic field changes from a Poisson distribution to the Wigner surmise as the magnetic field is increased.

---

smaller than two, and is satisfied in our case [106].

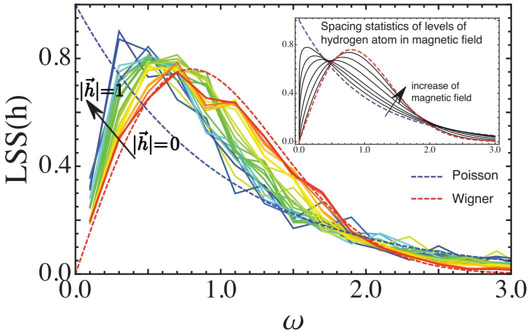

Figure 3.9: Behavior of the LSS of a granular system when h is changing from 0 to 1. The inset shows the so-called Brody distribution [111], which is an interpolating function between the Poisson and the Wigner distribution.

The presence of magnetic field spits the energy levels, giving rise to an increase in their collision, *i.e.*, increase in level interaction. For our systems it is the other way around — the perturbation makes modes collide and jump into the complex plane. This depletion of levels is responsible for less interactions between levels.

Our ultimate goal in this Section is to derive the scaling of the localization length with the system size by using the knowledge and tools of RMT. To do this, we need to relate our perturbation parameter $|\vec{h}|$ (that is directly connected with the localization length) with the typical frequency with which levels collide. To do this, we follow the RMT prescription in reference [106].

Generally speaking, our starting point is a Hamiltonian H_0, which is perturbed so that the new Hamiltonian has the structure $H(\lambda) = H_0 + \lambda V$, where λ is the perturbation parameter. According to RMT, mean temporal distance between two subsequent collisions of a level with its neighbors, *i.e.*, collision time λ_{coll}, should scale as some power of the number of levels. To find the scaling exponent one has to find the so-called *typical level velocity* and then the simple estimate for the collision parameter is:

$$\lambda_{coll} \approx \frac{mean\ level\ spacing}{typical\ level\ velocity}, \tag{3.4}$$

where the typical level velocity v is defined as:

$$v^2 = \overline{v_l^2} = \overline{\langle u^l|V|u^l\rangle^2}. \tag{3.5}$$

The average in previous equation is taken over an ensemble.

Following the general prescription, in order to calculate the collision parameter for the case of the spectrum of granular systems, we have to apply methods of the perturbation theory: The dynamical matrix $\hat{D}$ of our system is a sparse random matrix that is Hermitian (as mentioned before). When we introduce the asymmetric perturbation into the matrix (making sure that the diagonal is unchanged), our new matrix $\hat{M}$ is of the following form:

$$\begin{pmatrix}
\varepsilon_{11}^{x,x} & \varepsilon_{12}^{x,y} & \cdot & \cdot & \cdot & \cdot & \cdot & \cdot \\
\varepsilon_{21}^{y,x} & \varepsilon_{22}^{y,y} & \cdot & \cdot & \cdot & \cdot & \cdot & \cdot \\
\cdot & \cdot & \varepsilon_{33}^{x,x} & \varepsilon_{34}^{x,y} & c_{i,j}^{x,x} e^{\vec{h}\cdot\vec{r}_{i,j}} & c_{i,j}^{x,y} e^{\vec{h}\cdot\vec{r}_{i,j}} & \cdot & \cdot \\
\cdot & \cdot & \varepsilon_{43}^{y,x} & \varepsilon_{44}^{y,y} & c_{i,j}^{y,x} e^{\vec{h}\cdot\vec{r}_{i,j}} & c_{i,j}^{y,y} e^{\vec{h}\cdot\vec{r}_{i,j}} & \cdot & \cdot \\
\cdot & \cdot & \cdot & \cdot & \cdot & \cdot & \cdot & \cdot \\
\cdot & \cdot & c_{j,i}^{x,x} e^{\vec{h}\cdot\vec{r}_{j,i}} & c_{j,i}^{x,y} e^{\vec{h}\cdot\vec{r}_{j,i}} & \cdot & \cdot & \cdot & \cdot \\
\cdot & \cdot & c_{j,i}^{y,x} e^{\vec{h}\cdot\vec{r}_{j,i}} & c_{j,i}^{y,y} e^{\vec{h}\cdot\vec{r}_{j,i}} & \cdot & \cdot & \cdot & \cdot \\
\cdot & \cdot & \cdot & \cdot & \cdot & \cdot & \cdot & \cdot \\
\cdot & \cdot & \cdot & \cdot & \cdot & \cdot & \cdot & \cdot \\
\cdot & \cdot & \cdot & \cdot & \cdot & \cdot & \cdot & \cdot
\end{pmatrix}$$

By definition $\vec{r}_{j,i} \equiv -\vec{r}_{i,j}$ and $c_{i,j} \equiv c_{j,i}$. Taking this into account, we can rewrite our matrix as:

$$\begin{pmatrix}
\varepsilon_{11}^{x,x} & \varepsilon_{12}^{x,y} & \cdot & \cdot & \cdot & \cdot & \cdot & \cdot \\
\varepsilon_{21}^{y,x} & \varepsilon_{22}^{y,y} & \cdot & \cdot & \cdot & \cdot & \cdot & \cdot \\
\cdot & \cdot & \varepsilon_{33}^{x,x} & \varepsilon_{34}^{x,y} & c_{i,j}^{x,x} e^{\vec{h}\cdot\vec{r}_{i,j}} & c_{i,j}^{x,y} e^{\vec{h}\cdot\vec{r}_{i,j}} & \cdot & \cdot \\
\cdot & \cdot & \varepsilon_{43}^{y,x} & \varepsilon_{44}^{y,y} & c_{i,j}^{y,x} e^{\vec{h}\cdot\vec{r}_{i,j}} & c_{i,j}^{y,y} e^{\vec{h}\cdot\vec{r}_{i,j}} & \cdot & \cdot \\
\cdot & \cdot & \cdot & \cdot & \cdot & \cdot & \cdot & \cdot \\
\cdot & \cdot & c_{i,j}^{x,x} e^{-\vec{h}\cdot\vec{r}_{i,j}} & c_{i,j}^{x,y} e^{-\vec{h}\cdot\vec{r}_{i,j}} & \cdot & \cdot & \cdot & \cdot \\
\cdot & \cdot & c_{i,j}^{y,x} e^{-\vec{h}\cdot\vec{r}_{i,j}} & c_{i,j}^{y,y} e^{-\vec{h}\cdot\vec{r}_{i,j}} & \cdot & \cdot & \cdot & \cdot \\
\cdot & \cdot & \cdot & \cdot & \cdot & \cdot & \cdot & \cdot \\
\cdot & \cdot & \cdot & \cdot & \cdot & \cdot & \cdot & \cdot \\
\cdot & \cdot & \cdot & \cdot & \cdot & \cdot & \cdot & \cdot
\end{pmatrix}$$

The next step is to decompose our *perturbed* matrix $\hat{M}$ into $\hat{M} = \hat{D} + \delta\hat{M}$, where $\hat{D}$ is the original dynamical matrix, and $\delta\hat{M}$ is our perturbation which we define as:

$$\delta\hat{M} = \hat{M} - \hat{D} \tag{3.6}$$

Written in a matrix form, $\delta\hat{M}$ looks like:

$$\begin{pmatrix}
0 & 0 & . & . & . & . & . & . \\
0 & 0 & . & . & . & . & . & . \\
. & . & 0 & 0 & c_{i,j}^{x,x}(e^{\vec{h}\cdot\vec{r}_{i,j}}-1) & c_{i,j}^{x,y}(e^{\vec{h}\cdot\vec{r}_{i,j}}-1) & . & . \\
. & . & 0 & 0 & c_{i,j}^{y,x}(e^{\vec{h}\cdot\vec{r}_{i,j}}-1) & c_{i,j}^{y,y}(e^{\vec{h}\cdot\vec{r}_{i,j}}-1) & . & . \\
. & . & . & . & . & . & . & . \\
. & . & c_{i,j}^{x,x}(e^{-\vec{h}\cdot\vec{r}_{i,j}}-1) & c_{i,j}^{x,y}(e^{-\vec{h}\cdot\vec{r}_{i,j}}-1) & . & . & . & . \\
. & . & c_{i,j}^{y,x}(e^{-\vec{h}\cdot\vec{r}_{i,j}}-1) & c_{i,j}^{y,y}(e^{-\vec{h}\cdot\vec{r}_{i,j}}-1) & . & . & . & . \\
. & . & . & . & . & . & . & . \\
. & . & . & . & . & . & . & . \\
. & . & . & . & . & . & . & .
\end{pmatrix}$$

We now proceed with the first order perturbation theory, since we want to find corrections to the energy, *i.e.*, the shifts of the eigenvalues $\delta\omega^2$ for $|\vec{h}| \neq 0$. In other words:

$$\delta\omega_l^2 = \langle u^l|\delta\hat{M}|u^l\rangle = \sum_{\langle i,j\rangle}^{dN} u_i^l u_j^l \delta M_{i,j}, \tag{3.7}$$

where this sum runs over all the i, j non-zero pairs in the $\delta\hat{M}$, and we take $\langle u^l|u^l\rangle = 1$. If we would expand the exponentials into Taylor series only to first order (we can do that now because $h \ll 1$ and $\vec{r}_{i,j}$ is just a number of order 1), our matrix elements would become $e^{\pm\vec{h}\cdot\vec{r}_{i,j}} - 1 \approx \pm\vec{h}\cdot\vec{r}_{i,j}$. The result of this expansion, to the fist order only, is that our perturbation matrix becomes *asymmetric*. This now implies that our sum is equal to zero: we have a sum of a product of a symmetric part $u_i^l u_j^l$ (since $u_j^l u_i^l = u_i^l u_j^l$), and a asymmetric part $\delta M_{i,j}$, that therefore gives $\sum A\cdot S = 0$. Let us then not restrict ourselves to first order in h at this step, and symmetrize the product. Then:

$$\delta\omega_l^2 = \sum_{\langle i,j\rangle} u_i^l u_j^l (\delta M_{i,j} + \delta M_{j,i}) = 2\sum_{\langle i,j\rangle} 2u_i^l u_j^l c_{i,j}\sinh^2(\vec{h}\cdot\vec{r}_{i,j}/2) \tag{3.8}$$

where this symmetrized sum goes over all non-zero elements in the upper diagonal part of the $\delta\tilde{M}$.

To be able to proceed with our calculation, we need to mention the "structure" of the eigenvectors. Simply, we can say that if a mode is extended (which is true for most of our modes), and our eigenvectors $|u^l\rangle$ are normalized, the individual displacements within an eigenvector, u_i^l, in d dimensions scale with the system size as $\sim 1/\sqrt{dN}$[2]. Therefore we can take $u_i^l u_j^l$ to be of order $1/N$. We will also assume that for nearest neighbors, the u_i^l's within a mode are correlated (of the same sign), and come from some symmetric-around-zero distribution. These assumptions are corroborated by the actual mode fields. In the end, assuming that the average distance

---

[2] we assume here effectively that the modes have a Participation Ratio which does not go down as a N^{-b} with $b > 0$

between the neighboring particles $\vec{r}_{i,j}$ is constant, and equal to $\vec{a}$, we get the following relation between the first energy correction and the perturbation parameter:

$$\delta\omega_l^2 \simeq \frac{1}{N}\sinh^2(\vec{h}\cdot\vec{a}/2)N \sim \sinh^2(\vec{h}\cdot\vec{a}/2). \tag{3.9}$$

Since we are considering only small h we can expand $\sin(h)$ into series, and get that $\delta\omega_l^2 \sim h^2$. We checked numerically how $\delta\omega_l^2$ scales, and in 1d and 2d we see scaling with h^2.

After deriving that $\delta\omega_l^2 \sim h^2$, we can now return to the equation for the typical level velocity, (3.5). Taking our perturbation to be h^2 in the lowest order, we calculate that $v^2 \sim 1$. This result we have checked for various system sizes in 1 and 2 dimensions.

At this point we should note that we did not average our results over an ensemble. The reason is that we assume that the individual displacements in an extended mode would scale as $1/\sqrt{N}$ in any ensemble member, and that an extended mode will be extended in practically all the ensemble members.

Coming back to our starting equation (3.4), and using the relation derived above, we can write that:

$$\lambda_{coll} = h_c^2 \approx \frac{mean\ level\ spacing}{typical\ level\ velocity} \sim \frac{1/N}{1} \implies h_c \sim N^{-1/2} = L^{-d/2}, \tag{3.10}$$

where we took for the mean level spacing $\overline{\Delta\omega} \sim 1/N$. Finally:

$$\bar{\xi} \sim L^{d/2}, \tag{3.11}$$

which is exactly the scaling that we observed! Fig. 3.10 shows that the $\bar{\xi} \sim L$ scaling is well obeyed for our two-dimensional packings for the extended modes in the range $\omega \lesssim 3$ (as noted before the quasi-localized modes obey $\bar{\xi} \simeq 0.3L$), while the high-frequency localized modes for $\omega \gtrsim 3.4$ have $\bar{\xi}$'s which are indeed essentially L-independent. More generally we propose:

$$\bar{\xi} \sim L^{d/2}/W, \tag{3.12}$$

where W is a measure of the effective disorder. For our gently prepared granular packings the strength of the disorder cannot easily be varied, and therefore we will explore this scaling in more detail in Section 3.6.

3.5.1 Distribution of large ξ's revisited

In this Section we will address the power-law scaling of the tail of the distribution of large ξ. As we already showed in Section 3.4.4, the distribution of large localization length (in the units of the average $\bar{\xi}$) has a power-law tail that goes like ξ^{-3}, independently of the distance of the packing to the jamming point (see Fig. 3.8). Using the results from previous Section, we now derive this scaling.

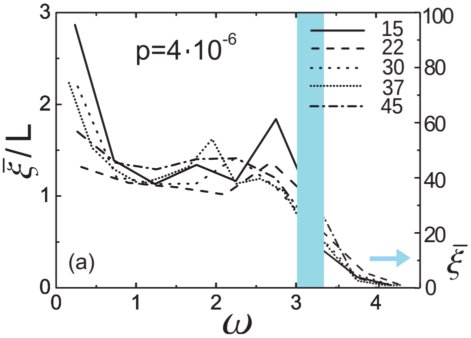

Figure 3.10: Finite size scaling for $p = 4 \cdot 10^{-6}$ and linear system size L ranging from 15 to 45, confirming that the extended states, where $\bar{\xi} \gtrsim L$, scale with L, while the high-frequency modes are, within the statistical error, L-independent.

As we elaborated extensively in previous Sections, when we turn on $h \equiv |\vec{h}|$, a certain number of modes starts colliding and jumping into the complex plane, whereas some of the remaining modes shift, *i.e.*, their spacing becomes smaller or bigger. When we increase h further, *i.e.*, $h \to h + \Delta h$, the following behavior of the modes can be observed: *(i)* modes that are already in the complex plane, continue moving in it; *(ii)* modes that approached close enough after the previous change of h, *i.e.*, are now at a distance $\lesssim \Delta h$, will now collide and jump into $\mathbb{C}$; *(iii)* the rest of the modes either comes closer to their neighbors, or moves further apart. We know from both theory (the analysis above) and numerics that $\delta\omega^2 \sim h^2$, so when we change h to $h + \Delta h$ our mode perturbation changes to:

$$\delta\omega_l^2 \sim h^2 \to h^2 + h\Delta h \equiv \delta\omega_l^2 + \Delta\delta\omega_l^2. \tag{3.13}$$

Let us for a moment step back and think about the modes that have large localization lengths. We know that these modes (in pairs) had to be very close to each other, because for a very small value of the perturbation parameter they already collided with their nearest neighbor. So, we can first ask the question what is the number of modes that pop into the complex plane (*i.e.*, that have their $\xi \equiv 1/h_c$) when we change h by Δh:

$$N_{h_c} \simeq v \int_{\epsilon}^{\epsilon+\Delta\epsilon} P_W(x)dx \sim \epsilon\Delta\epsilon, \text{ because } P_W(x) \sim x \text{ for } x \ll 1, \tag{3.14}$$

where P_W is the Wigner distribution. In the previous equation the *collision frequency* v, *i.e.*the factor that quantifies how many of the modes from $\Delta\epsilon$ interval did actually collide, is of the order of unity. It is important to note that only the linear part of the distribution is used (see Eq. (3.3)), and this part stays linear as h is increased and the distribution evolves towards the Poisson shape (see Fig. 3.9).

Finally let us write the density of the variable h_c (*i.e.*ξ): $P_{h_c} \sim \frac{\epsilon\Delta\epsilon}{\Delta h}$. According to the present consideration, a collision means that the modes found in the range $\Delta\epsilon$

move enough to cover this range, $\Delta\delta\omega^2 \simeq \Delta\epsilon$. Since $\Delta\delta\omega^2 \sim h\Delta h$, we have $\Delta\epsilon \sim h\Delta h$ which after integration gives us $\epsilon \sim h^2$. Now we can substitute all of the above into the expression for the density P_{h_c} and get:

$$P_{h_c} \sim h \cdot \epsilon \sim h^3 = \xi^{-3}, \tag{3.15}$$

which is exactly the result that we observed in our granular packings, see Fig. 3.8. As we shall see in later Sections, this behavior is very robust, and will appear again.

3.6 Exploring the method

This Section is devoted to the exploration of the method we used above to extract the localization length, [107, 108]. First, we will start with exploring in more detail how the length we calculate is related with the true, *intrinsic*, localization length of the modes. We will do this in $1d$ by studying a *disordered chain*, since it is much easier to reach the large system limit. Next, we will justify the proposed scaling of Eq. (3.12), by studying $2d$ *disordered hexagonal lattices*, since we can disentangle different types of disorder (see Section 3.1.2). In the end we will apply all the knowledge presented in this Chapter on *percolation clusters in* $2d$ as models of structurally disordered solids.

3.6.1 $1d$: disordered chain

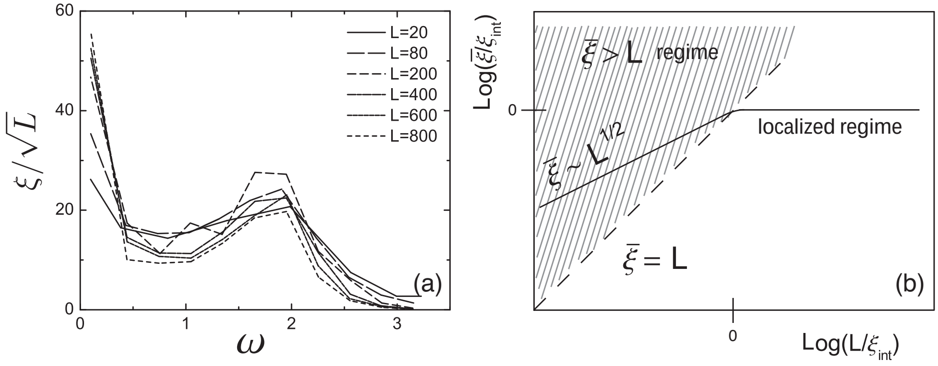

Figure 3.11: (a) Localization length as a function of vibrational frequency for a one-dimensional chain, rescaled with the square-root of the system size. L is in the range 20-800 particles. (b) Sketch of the proposed scaling regimes of the localization length. According to this, data in panel (a) falls in the shaded region, for which $\xi \sim L^{1/2}$.

We study disordered chain of particles with periodic boundary conditions, where the disorder is introduced only by varying the masses of the particles at each site. The spring constants k are all the same and equal to 1. We analyzed systems of different sizes and fixed amount of disorder (20% polydispersity in radii). As in the case of $2d$ granular packings, we extract the localization length of our $1d$ system using the method described in Section 3.2. Although working with $1d$ systems is less demanding CPU-time wise, all of our data is averaged only over 10 different realizations of disorder, since we need to repeat the diagonalization of the Dynamical Matrix many times (for each value of h), and that takes a long time.

The results obtained for a range of system sizes are shown in Fig. 3.11(a). The localization length is rescaled with $\sqrt{L}$, following our prediction, Eq. (3.12).[3] Within the statistical error we see a collapse of our data.

The main idea of this Section is to relate the localization length that we measure with the one for an infinitely large system. Therefore we will define ξ_{int} to be the *intrinsic localization length*, the localization length if we have the same physical system, but infinitely large. This means that when we study the system as a function of the system size L, we will get $\xi \simeq \xi_{int}$ for $L \gg \xi_{int}$, since our method does give the right localization length if the wave-functions are localized. At this point, we want to argue that there should be a crossover for $L \approx \xi_{int}$, after which we enter into the *intrinsic localization regime* for any $L > \xi_{int}$. This argument is sketched in panel (b) of Fig. 3.11.

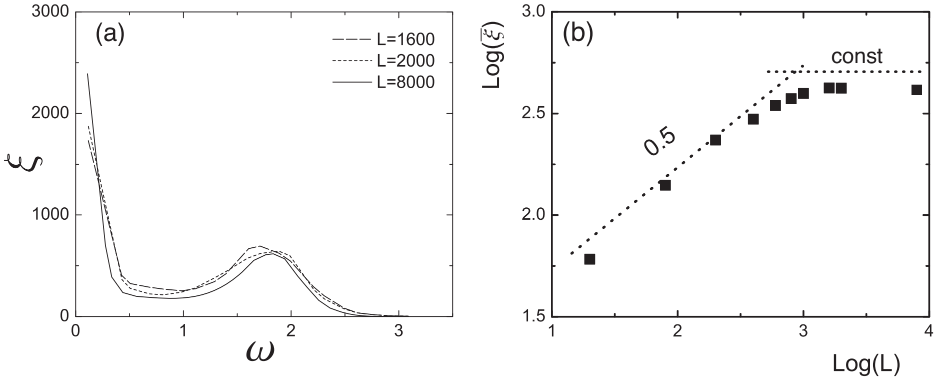

Figure 3.12: (a) Localization length as a function of vibrational frequency for a one-dimensional chain. L is in the range 1600-8000 particles. (b) Localization length $\bar{\xi}$ averaged over the spectrum, as a function of the system size L. Above $L \sim 1000$ the localization length we measure is the intrinsic one.

To test the previous statements, we performed simulations for a range of system sizes L. Some of the results are shown in Fig. 3.12(a). It is important to note that our localization curves fall on top of each other *without* any rescaling. In Fig. 3.12(b) we show the system averaged localization length (calculated with our method) as a

---

[3] Since the amount of disorder is fixed, the W parameter will not play a role in this analysis.

function of a system size. This data suggest that a crossover from the square-root behaviour is observed when we reach system size $L > 1000$. In these "large" systems, length that we measure is the true localization length!

We predicted and found a scaling $\xi \simeq AL^{1/2}$ in the regime $\xi \gtrsim L$. Since we expect a crossover to the localization regime when the *intrinsic* localization length obeys $\xi_{int} \simeq L$, this suggests that we can estimate infinite size localization length from the small system data simply as $\xi_{int} \simeq A^2$. Note that unfortunately for a $2d$ problem determining ξ_{int} from ξ, when $\xi \gtrsim L$, is not possible using this approach. However in $3d$, $\xi_{int} \simeq 1/B^2$ when $\xi \simeq BL^{3/2}$ as long as we are applying it to the localized modes, above the mobility edge. If ξ_{int} becomes infinite, our method gives an unbound value for ξ, as we checked in $1d$ without disorder. We expect similar behavior for truly extended modes in $3d$.

The numerical simulations to check/confirm the connection between ξ_{int} and ξ can in principle be repeated for any dimension larger than 1. But, as we pointed out before, checking this for the $2d$ granular systems, is extremely hard, since achieving an order of magnitude in linear system size requires our computer programs to run for over a year.

3.6.2 $2d$: disordered hexagonal lattice

As already mentioned above, disentangling different types of disorder in the case of granular packings is quite hard. In order to test our prediction of the scaling of the localization length with the amount of disorder we have to move to another system, where this can be controlled. Therefore we studied geometrically ordered hexagonal lattices where the disorder is introduced by varying the masses of the particles at each site (20% polydispersity in the radii). The spring constants k are all the same and equal to 1.

For illustrative purposes, in Fig. 3.13 we show the density of states of disordered hexagonal lattices, with different amounts of disorder. The linear system size is $L = 31$. Increasing the amount of disorder causes an increase of the number of high-frequency modes, on account of a decrease of mid-frequency ones. This rearrangement of the modes in the spectrum "washes out" the peaks given by the lattice band structure.

It is instructive to note here that the shape of the $D(\omega)$ for a very compressed granular packing, shown in Fig. 3.2, resembles the disordered hexagonal ones in the previous plot. In the granular case the average coordination number $Z \sim 5.2$, slowly approaching the hexagonal lattice ("classical $2d$ solid") coordination, $Z \equiv 6$.

The main result of this Subsection is shown in Fig. 3.14: In (a) we plot $\bar{\xi}(\omega)/L$ for various system sizes and amounts of disorder. Groups of collapsed curves have the same amount of disorder, *i.e.*, the same width of the radii distribution! In order to test our scaling prediction Eq. (3.12), we rescaled the localization length with the amount of the disorder W (in this case it is the half width of the distribution of the radii). As Fig. 3.14(b) shows, we obtain very good data collapse at all but the highest

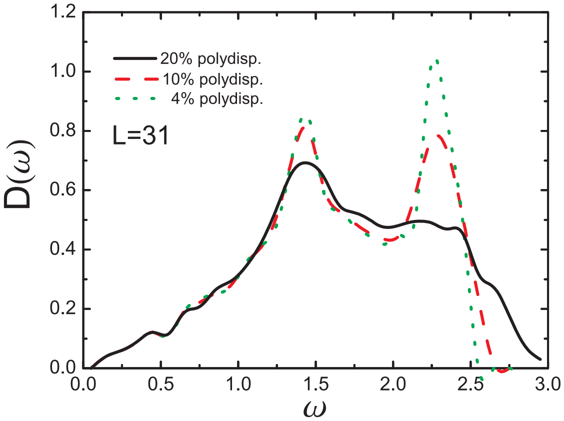

Figure 3.13: The density of states for disordered hexagonal lattice. Different curves are for different amounts of polydispersity in particle radii.

frequencies. Note also that for small amount of disorder, we have $\bar{\xi} \gg L$.

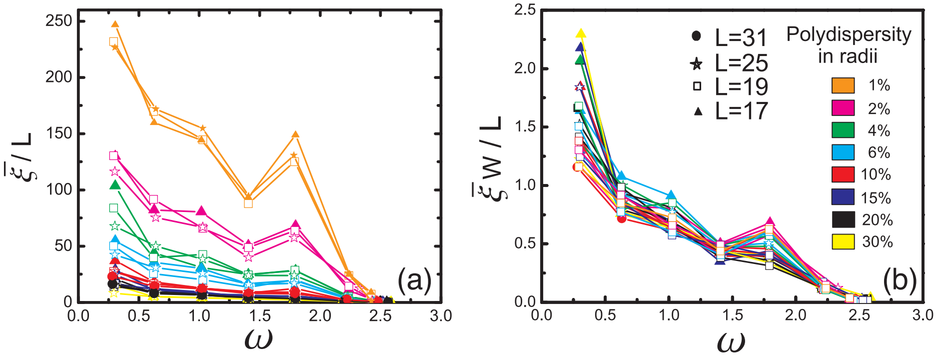

Figure 3.14: (a) $\xi(\omega)/L$ for different system sizes of 2d disordered hexagonal lattice and fixed disorder due to polydispersity in radii (b) Collapse of data consistent with Eq. (3.12).

We have commented before, that the scaling of the tail of the distribution of large ξ (that we observed and derived) is robust. To support this, in Fig. 3.15, we plot $P(\xi/\bar{\xi})$ for different amounts of disorder. As one can see the large localization lengths follow the $(\xi/\bar{\xi})^{-3}$ scaling as well.

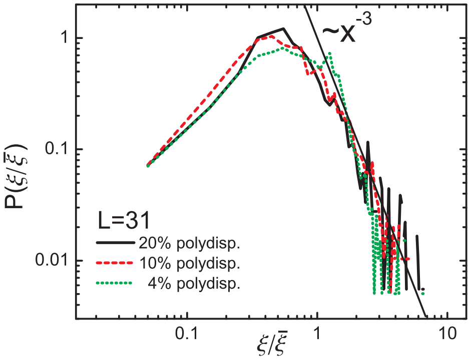

Figure 3.15: Log-log plot of the distribution of ξ's for different amounts of disorder in the hexagonal lattice. Solid black line shows the power law decay derived in Section 3.5.1.

3.6.3 Percolation clusters

One of the most used models of structurally disordered solids is the *percolation* model [112]. The simplest way to understand this model is to start from a square lattice where each site is occupied randomly with probability p, and is consequently empty with probability $p-1$[4]. Examples of percolation on a square lattice for four different probabilities p are shown in Fig. 3.16. For low probabilities (p less than in Fig. 3.16(a)) occupied sites are isolated from each other, or they form clusters that are small compared to the system size. As the probability is increased the average size of the clusters grows, Fig. 3.16(a), and at some threshold concentration p_c a large cluster forms that spans the system, *i.e.*, it percolates from one edge of the system to the other. In Fig. 3.16(b) we show such a cluster just above the threshold value p_c. When the probability p is increased further, the density of this so-called "infinite cluster" [5] increases as well, Fig. 3.16(c-d).

It is intuitively clear that the percolation threshold strongly depends on the dimensionality of the problem and the coordination of the lattice considered. For the two-dimensional case of site percolation on a square lattice ($Z=4$) $p_c \approx 0.592746$.

Localization behavior of vibrational modes in the infinite percolation cluster above p_c was studied in detail in $2d$ and $3d$ by Bunde and collaborators in [105]. By looking at the second moment of the level spacing distribution of the energy levels, they found that all eigenstates are localized in $d=2$. In this Subsection we are going to address the vibrational behavior of percolation clusters using the method presented in Section 3.2 and actually calculate the localization length.

We simulate $2d$ site percolation clusters above p_c on a square lattice with periodic

---

[4] As an illustration one can think about occupied sites as electrical conductors and empty ones as insulators. In this way the metal-insulator transition is mapped onto a percolation problem.

[5] It is called "infinite" because its size diverges in the thermodynamic limit.

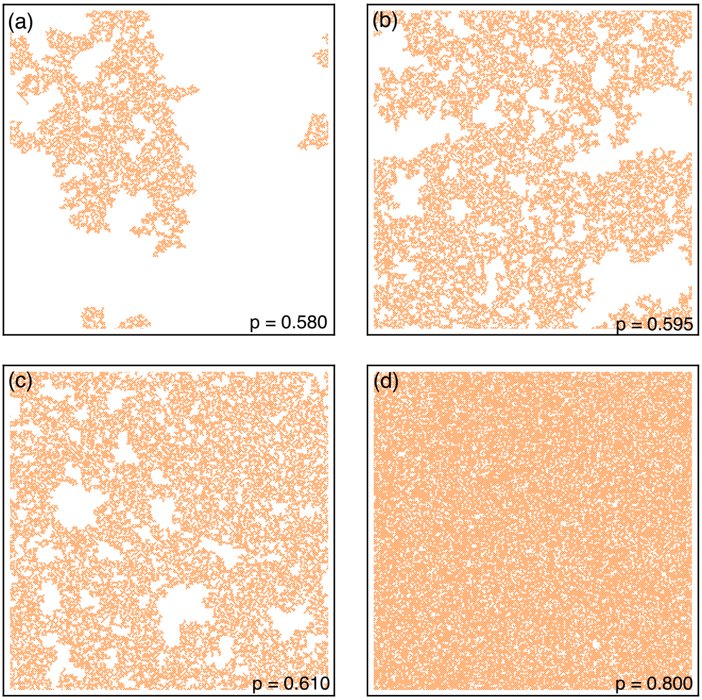

Figure 3.16: Percolation clusters on the square lattice at probability (a) $p = 0.580$, (b) $p = 0.595$, (c) $p = 0.610$ and (d) $p = 0.800$. Going from (a) to (d) one can see how the size of the cluster grows and becomes more dense.

boundary conditions using the Leath algorithm [113]. After making the clusters, the dynamical matrix for each sample is generated assuming equal masses of the each occupied site, and equal nearest neighbor coupling $k \equiv 1$. Effectively, this model is not a proper dynamical model like we studied for jamming, it is essentially the scalar diffusion problem on a percolating lattice.

In Fig. 3.17 we show the density of states of infinite percolation clusters made with different probabilities p above p_c. The general shape of the spectrum resembles the one for disordered jammed packings above jamming (see Fig. 3.2) — as the threshold p is increased above p_c low frequency part of the density of states goes to zero in a linear-like fashion, Fig. 3.17(a).

Following [105], we rescale both $D(\omega)$ with $\omega^{d_s-1}$and ω with $(p-p_c)^{d_w\nu/2}$, where $d_s = 2d_f/d_w$ is the spectral dimension, d_f is the fractal dimension, d_w is the anomalous diffusion exponent and ν is the correlation length exponent ($\nu = 4/3$ in $2d$). The arguments for this scaling can be found in [105] and references therein. In this way DOS of different percolating systems separate into two groups: *phonons*, where the

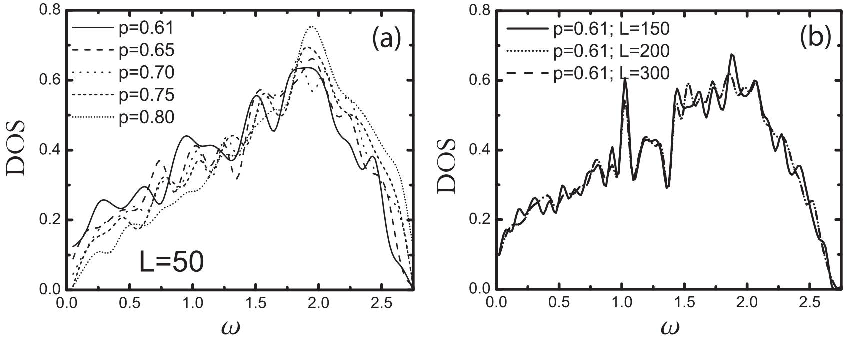

Figure 3.17: (a) Density of states of infinite site percolation clusters at several probabilities p above p_c and fixed system size $L = 50$. (b) Density of states for infinite site percolation clusters for a fixed probability $p = 0.61$ and varying system sizes.

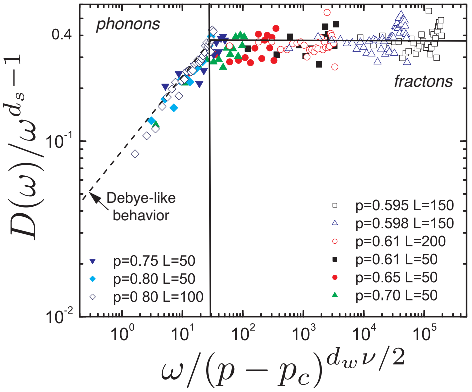

Figure 3.18: Rescaled density of states for several probabilities p and several system sizes L. Note how the rescaling separates two different types of modes: phonons and fractons.

low-frequency part of the density of states follows the Debye law, and *fractons*, the low-frequency part of the density of states scales anomalously with ω. Collapse of our data for several probabilities p and several system sizes L are shown in Fig. 3.18.

To get an intuition on the differences in the appearance of fracton and phonon modes, in Fig. 3.19 we are showing a few examples from different parts of the spectrum.

The main result of this Subsection is shown in Fig. 3.20 where we plot the average localization length $\bar{\xi}$ as a function of eigenfrequency ω for percolation clusters at different probabilities p and different system sizes L. Figs. 3.20(a-c) address the

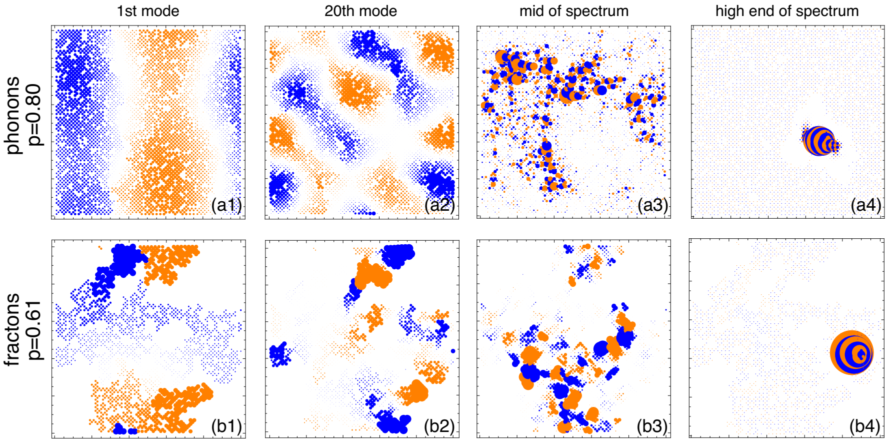

Figure 3.19: Examples of eigenmodes for systems of linear size $L = 100$ and two different probabilities: in (a1-a4) $p = 0.80$, and in (b1-b4) $p = 0.61$. The radii of the disks in the plots are proportional to the amplitude of the oscillation and the color shows the phase.

localization behavior of fractons and (d-e) the localization behavior of phonons.

Indeed as indirectly found by Bunde *et al.*, we also find that the vibrational modes are localized within our finite systems, *i.e.*, we expect that we are measuring the intrinsic localization length of these modes. It is interesting that the localization behavior of fractons and phonons is different. In the case of fractons the values of ξ are independent of the system size L as one expects if $\xi_{int} \ll L$. However the phonons show $\xi \sim L$ — in practice we find that $\xi \simeq L/2$. This is not unreasonable for an extended mode which takes on values of both sign in a box with periodic boundary conditions (for a sign-wave like mode which just fits in the box, the correlation function reaches a minimum over a distance $L/2$). Also one should keep in mind that while all definitions of the localization length agree as long as $\xi \ll L$, the precise value of ξ depends on the definition, once ξ is of order L.

We mention in passing that the scaling of the tail of the distribution of large localization lengths is consistent with the scaling we found for granular packings and $2d$ disordered hexagonal lattice.

Bunde *et al.*finds that in $3d$ the localization-delocalization transition occurs somewhere in the fracton regime, so that there are delocalized phonons and delocalized fractons at all probabilities $p > p_c$. It would be interesting to repeat our calculation of the localization length for $3d$ clusters and see if the different scaling of ξ with L can distinguish between the different types of extended modes.

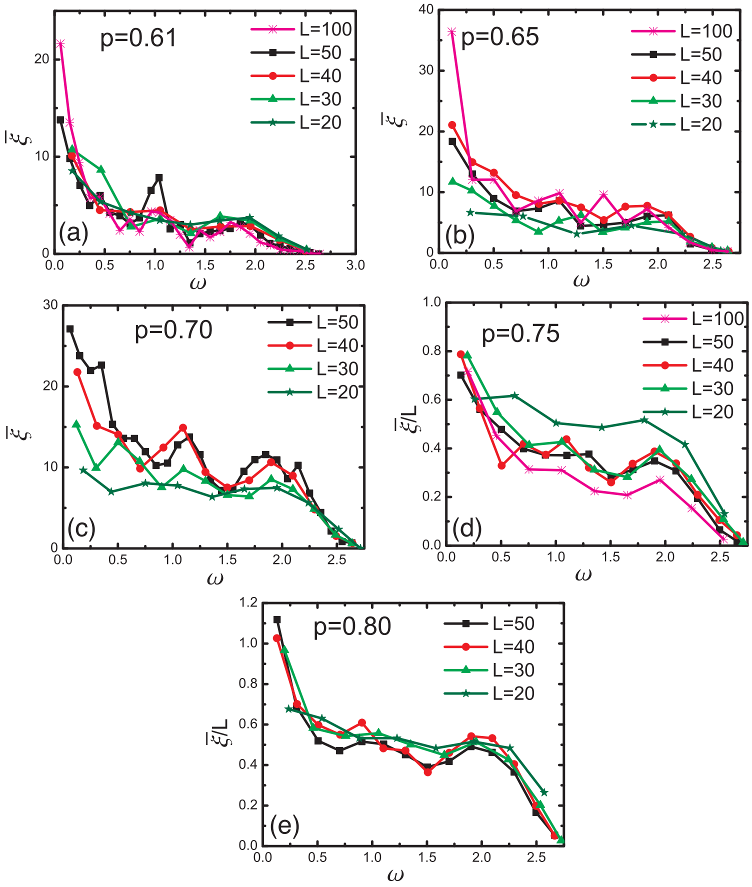

Figure 3.20: $\xi(\omega)$ for different system sizes of percolation clusters at several probabilities. For fractons, our method measures the intrinsic localization length: in (a), (b) and (c) the localization length we measure does not scale with the system size — we measure the intrinsic localization length of fracton modes! In (d) and (e) we show $\bar{\xi}/L$ for phonons we find at large probabilities. Note that phonons behave as in granular systems and 1d and 2d disordered lattice problems studied in previous Sections.

3.7 Conclusions

In this Chapter we have introduced a new method, motivated by previous studies of non-Hermitian quantum problems [107,108], which allows an analysis of localization in phonon spectrum, including the regime $\bar{\xi} \gtrsim L$ when the eigenmodes are extended within the finite systems we can study. The method is especially relevant for granular packings, where $\bar{\xi} \gtrsim L$ throughout most of the frequency range, since even in this regime our method gives different results depending on the amount of disorder. The disappearance of the quasi-localized low-frequency modes as we approach the jamming point by lowering the pressure is quite intriguing and their role in the response of the system is to be explored in the future.

A few final remarks are in order. *(i)* Our method allows us to determine which type of disorder (mass disorder, bond disorder or geometrical disorder) plays the dominant effect in the localization behavior. *(ii)* The results for $\bar{\xi}(\omega)$ in finite system typically show an upswing for small ω, except at the largest pressures; whether this is a finite system analogue of the well known $\omega \to 0$ divergence in infinite $2d$ systems [5] is unclear to us. *(iii)* The states with large but finite localization lengths at low frequency that we find at high pressures (see Fig. 3.7(a)) are intriguing. It will be interesting to see if these states persist in the presence of the entropic interactions at finite temperature. *(iv)* Diffusion on percolation lattices is also an appealing model system to apply the method to: close to the percolation threshold most eigenmodes are truly localized and thus have $\xi \ll L$, while away from the percolation threshold there is a crossover to the regime where $\bar{\xi} \geq L$.